Achieving tunable Kerker-type invisibility for a radiation-enhanced electrically small antenna

Peiqi Chen,[1] Qiuyue Nie,[1,2,*] Zhonglin Zhang,[2] Bowen Li,[3] Weishuo Li,[1] and Xin Ai[1]
[1]*School of Electrical Engineering and Automation, Harbin Institute of Technology, Harbin 150001, China*
[2]*Laboratory for Space Environment and Physical Science, Harbin Institute of Technology, Harbin 150001, China*
[3]*School of Physics, Harbin Institute of Technology, Harbin 150001, China*

(Received 5 May 2022; accepted 15 August 2022; published 21 September 2022)

Low-temperature gaseous plasmas exhibit great potential in designing tunable and reconfigurable electromagnetic devices. In this paper, based on an overdense-underdense core-shell plasma structure, tunable Kerker-type invisibility for a radiation-enhanced electrically small antenna is achieved, where dominant scattering direction can be mutated between backward and forward while omnidirectional invisibility and signal enhancement are maintained. Moreover, by electromagnetic multipole decompositions, it is shown that the underdense outer plasma with a negative polarizability is able to weaken the strength and modulate the phase of the electric dipolar scattering component (a_1), while the magnetic dipolar term (b_1) nearly remains unchanged. Consequently, quasi-first and -second Kerker conditions are fulfilled near the cutoff band of a_1.

DOI: 10.1103/PhysRevE.106.035207

I. INTRODUCTION

In recent decades, low-temperature gaseous plasmas have received increasing attention in manipulating electromagnetic (EM) waves from microwave to terahertz [1–8]. This trend lies in the fact that plasma can be regarded as a subset of metamaterials in two aspects. One is that plasma's relative permittivity can be continuously and dynamically tuned in a broad range by changing external parameters [9], such as discharge power, pressure, gas species, etc. Particularly, plasmas of weak collision can flexibly function as ENG (epsilon-negative), ENZ (epsilon-near-zero), or ELP (epsilon-low-positive) media under different electron densities. The other is that, when taking specific subwavelength structures into account, plasma's electromagnetic characteristics become completely different from a bulk one [9,10]. Collectively, these two features endow the plasma with great potential in designing various tunable and reconfigurable EM devices, including filters [11,12], waveguides [13,14], antennas [3–5], etc.

On the other hand, modern wireless communication systems are developed towards miniaturization, portability, and versatility. As key components, the electrically small antennas (ESAs) are not only required to be efficient, but also desirable with low and reconfigurable detectability for practical applications. In the meantime, the rapid advancement in nanophotonics and plasmonics has enabled controlling EM waves more flexibly and efficiently at the subwavelength scale. Such principles and techniques can then be adapted to the microwave frequency regime when normalized key parameters (e.g., size, permittivity, and permeability) remain the same as those in visible bands of EM waves, which are conducive to integrating the aforementioned two functions into one system by means of plasmas. For the former, surface plasmon subwavelength optics [15–17] has opened a new front for enhancing the intensity of light in the near- or the far field. Correspondingly, recent studies have demonstrated that the radiation efficiency of ESAs can be intensified up to 20 dB from MHz to GHz by overdense or ENG plasma both by experiments [4,5,18,19] and simulations [20–24]. For the latter, Kerker effect [25–33] and plasmonic cloaking [34–40] are powerful tools to control or reshape the scattering pattern of a target illuminated by EM waves. Specifically, Kerker effect is widely applied for reconfiguring scattering patterns or directional scattering control, where backward or forward scattering can be substantially suppressed by the constructive or destructive interference between electric and magnetic scattering components. Moreover, plasma's ELP characteristics make it an ideal candidate in implementing plasmonic cloaking, which is advantageous over conventional absorption-based plasma stealth [41] since plasmonic cloaking is a volumetric effect operated in a nonresonant and nonabsorption manner and thus is able to strike a balance between reducing a target's detectability and maintaining its communication capability [35]. However, two key issues need to be resolved to achieve the synergism between signal enhancement and reconfigurable invisibility: (1) the compatibility between plasma-based enhancement effect and invisibility induced by plasmonic cloaking in different directions remains unclear; and (2) most existing research aims to fulfill Kerker effect in or near the resonant regime by introducing artificial magnetic resonances [28–33]. In such a situation, even though scattering in a certain direction is reduced, overall scattering efficiency is however greatly enhanced, which inevitably limits its applications in invisibility.

Therefore, in this paper, we firstly investigate the compatibility between signal enhancement and invisibility induced by plasmonic cloaking in three crucial directions, namely, forward, spatially averaged, and backward based on an ENG-ELP core-shell plasma system. On that basis, the possibility to extend the scope of Kerker effect into the invisibility regime is unveiled drawing on Mie theory. Our results not only provide

*nieqiuyue@hit.edu.cn

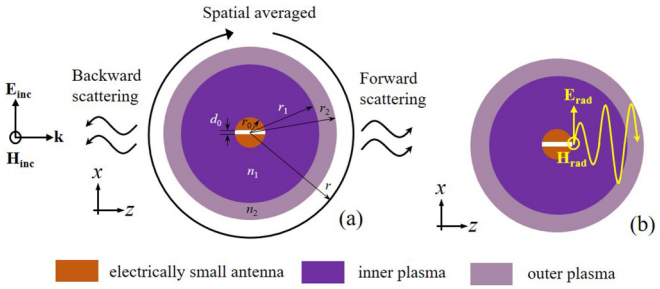

FIG. 1. Schematics of the simulation model (x-z cross section) for (a) directional scattering control, and (b) signal enhancement.

a perspective to understand the implementation of Kerker effect in the invisibility regime, but also offer a referential path to design next-generation state-of-the-art stealth and sensing equipment.

II. SIMULATION MODEL

The x-z cross section of the simulation model, with the y-direction perpendicular to the view, by COMSOL MULTIPHYSICS [42] (version 5.4) is schematically shown in Fig. 1. From inside to outside, it consists of a coaxially fed spherical electrically small antenna (brown part with a radius of $r_0 = 0.6\,\text{cm}$, a feed gap of $d_0 = 0.1\,\text{cm}$, and a driving voltage of $V_0 = 1\,\text{V}$), an inner plasma shell (dark purple part with a thickness of $d_{\text{in}} = r_1 - r_0$ and an electron density of n_1, for signal enhancement) and an outer plasma shell (light purple part with a thickness of $d_{\text{out}} = r_2 - r_1$ and an electron density of n_2, for invisibility). The relative permittivity of the inner and outer plasmas is approximated by ($e^{j\omega t}$ time dependence is assumed)

$$\varepsilon_{\text{pr}}(\omega, \omega_{\text{pe}}) = 1 - \frac{\omega_{\text{pe}}^2}{\omega^2 + \nu^2} - j\frac{\omega_{\text{pe}}^2 \nu}{\omega(\omega^2 + \nu^2)}, \tag{1}$$

where ω is the angular frequency of EM waves interacting with plasmas, ω_{pe} is the plasma frequency (with ω_{in} and ω_{out} for the inner and outer plasma shells, respectively), and υ is the electron momentum transfer collision frequency (0.1 GHz). Additionally, the frequencies of detecting and communicating waves are 0.6 GHz (P band) and 1 GHz (L band), respectively, and both of them propagate along the z direction with an x-polarized electric field component.

To reveal the directional scattering characteristics of such a system, we define three different radar cross sections: normalized backward RCS ($\text{RCSB}_{\text{norm}}$), normalized forward RCS ($\text{RCSF}_{\text{norm}}$), and normalized average bistatic RCS ($\text{RCSAv}_{\text{norm}}$). They are represented as

$$\text{RCSB}_{\text{norm}} = 10\log_{10}(\text{RCSB}_{\text{wp}}/\text{RCSB}_{\text{ip}}), \tag{2}$$

$$\text{RCSF}_{\text{norm}} = 10\log_{10}(\text{RCSF}_{\text{wp}}/\text{RCSF}_{\text{ip}}), \tag{3}$$

$$\text{RCSAv}_{\text{norm}} = 10\log_{10}\left(\frac{\sum_1^l \text{RCSbi}_{\text{wp}}/l}{\sum_1^l \text{RCSbi}_{\text{ip}}/l}\right), \tag{4}$$

where the subscript "wp" stands for "with two plasma shells;" "ip" designates "with the inner plasma shell only;" and "l" represents the number of discrete calculation points along a spherical surface with a radius $r > r_2$ [Fig. 1(a)] in simulation. Besides, the normalized radiation gain of the antenna is defined as

$$P_{\text{gain}} = 10\log_{10}(P_{\text{wp}}/P_{\text{np}}), \tag{5}$$

where the footnote "np" denotes "with no plasma shells."

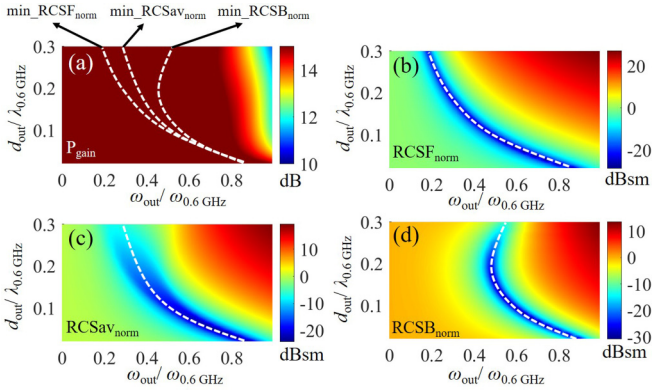

FIG. 2. Color maps of (a) P_{gain}, (b) $\text{RCSF}_{\text{norm}}$, (c) $\text{RCSAv}_{\text{norm}}$, and (d) $\text{RCSB}_{\text{norm}}$ under different normalized outer plasma parameters ($d_{\text{out}}/\lambda_{0.6\,\text{GHz}}$ and $\omega_{\text{out}}/\omega_{0.6\,\text{GHz}}$).

III. RESULTS AND DISCUSSION

As plasma is supposed to be overdense and of subwavelength for effective radiation intensification [35], for simplicity, the electron density and thickness of inner plasma are set as $5 \times 10^{16}\text{m}^{-3}$ ($\omega_{\text{in}}/\omega_{1\,\text{GHz}} = 2.01$) and 3 cm ($d_{\text{in}}/\lambda_{1\,\text{GHz}} = 0.1$), where an initial radiation gain (enhanced by inner plasma only, P_{gain0}) of ~15 dB can be obtained. On this basis, the characteristics of P_{gain}, $\text{RCSF}_{\text{norm}}$, $\text{RCSAv}_{\text{norm}}$, and $\text{RCSB}_{\text{norm}}$ under different normalized outer plasma parameters ($d_{\text{out}}/\lambda_{0.6\,\text{GHz}}$ and $\omega_{\text{out}}/\omega_{0.6\,\text{GHz}}$) are shown in Figs. 2(a)–2(d). For signal enhancement [Fig. 2(a)], since the outer plasma is underdense for communication signals ($\omega_{\text{out}}/\omega_{0.6\,\text{GHz}} < 1 \Leftrightarrow \omega_{\text{out}}/\omega_{1\,\text{GHz}} < 0.6$), it exerts a minute negative impact on P_{gain0} and thus a positive P_{gain} (>10 dB) is maintained both in the **E** plane and **H** plane, as demonstrated by the double arrows in Figs. 3(a) and 3(b). For invisibility, it can be seen that optimal $\text{RCSF}_{\text{norm}}$, $\text{RCSAv}_{\text{norm}}$, and $\text{RCSB}_{\text{norm}}$ (white dashed curves) are reachable where the relative outer plasma frequency is less than unity, and thus all of them are compatible with signal enhancement. However, there also exist several differences among them. Firstly, it can be observed that the three RCSs are achieved under different outer plasma parameters. Specifically, for a fixed thickness of the outer plasma shell, the minimums of $\text{RCSF}_{\text{norm}}$ ($\text{min\_RCSF}_{\text{norm}}$), $\text{RCSAv}_{\text{norm}}$ ($\text{min\_RCSAv}_{\text{norm}}$), and $\text{RCSB}_{\text{norm}}$ ($\text{min\_RCSB}_{\text{norm}}$) are obtained in sequence with the increase of $\omega_{\text{out}}/\omega_{0.6\,\text{GHz}}$. And, their discrepancy becomes more evident when increasing d_{out}. Secondly, only does $\text{min\_RCSB}_{\text{norm}}$ have a turning point where $\omega_{\text{out}}/\omega_{0.6\,\text{GHz}} \sim 0.5$ and $d_{\text{out}}/\lambda_{0.6\,\text{GHz}} \sim 0.2$. In other words, under a fixed ω_{out}, two values of d_{out} can be found for backward invisibility. By contrast, for $\text{min\_RCSF}_{\text{norm}}$ and $\text{min\_RCSAv}_{\text{norm}}$, the thicker the outer plasma shell is, the less dense it should be. Lastly, the

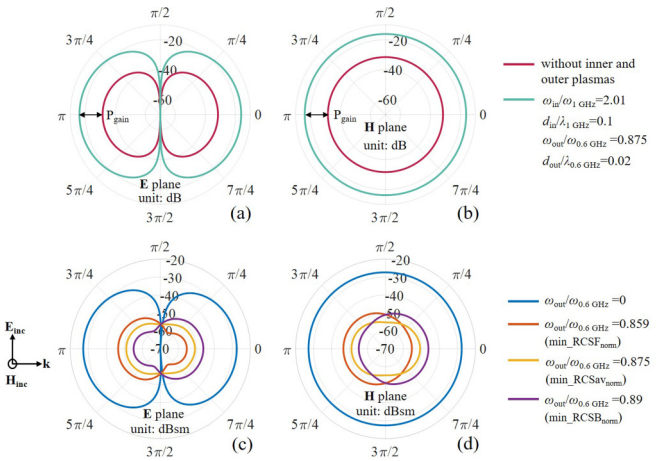

FIG. 3. P_{gain} in the **E** plane (a) and **H** plane (b), where the red curve stands for without inner and outer plasmas and the green curve denotes covering two plasma layers with $\omega_{in}/\omega_{1\,GHz} = 2.01$, $d_{in}/\lambda_{1\,GHz} = 0.1$, $\omega_{out}/\omega_{0.6\,GHz} = 0.875$, and $d_{out}/\lambda_{0.6\,GHz} = 0.02$; bistatic radar cross sections in the **E** plane (c) and **H** plane (d) with $d_{out}/\lambda_{0.6\,GHz} = 0.02$, where blue, orange, yellow, and purple lines designate $\omega_{out}/\omega_{0.6\,GHz} = 0$, $\omega_{out}/\omega_{0.6\,GHz} = 0.859$ (min_RCSF$_{norm}$), $\omega_{out}/\omega_{0.6\,GHz} = 0.875$ (min_RCSAv$_{norm}$), and $\omega_{out}/\omega_{0.6\,GHz} = 0.89$ (min_RCSB$_{norm}$).

effective invisibility bandwidth of RCSAv$_{norm}$ is larger than that of RCSF$_{norm}$ and RCSB$_{norm}$.

In addition, of particular interest is that with the decrease of d_{out}, min_RCSF$_{norm}$, min_RCSAv$_{norm}$, and min_RCSB$_{norm}$ tend to coincide. That is to say, when d_{out} is sufficiently small, the omnidirectional invisibility plays a dominate role, while a nuanced tuning of ω_{out} will lead to a drastic change of scattering patterns. For example, when $d_{out}/\lambda_{0.6\,GHz} = 0.02$, bistatic radar cross sections in the **E** plane and **H** plane for min_RCSF$_{norm}$ ($\omega_{out}/\omega_{0.6\,GHz} = 0.859$), min_RCSAv$_{norm}$ ($\omega_{out}/\omega_{0.6\,GHz} = 0.875$), and min_RCSB$_{norm}$ ($\omega_{out}/\omega_{0.6\,GHz} = 0.89$) are shown in Figs. 3(c) and 3(d). It can be observed that a slight increase of $\omega_{out}/\omega_{0.6\,GHz}$ from 0.859 to 0.89 results in the alternation of dominant scattering direction from backward to forward while invisibility in nearly all directions is maintained.

On the other hand, according to the Mie theory [43], directional scattering efficiencies can also be expressed as a series of expansions of Mie coefficients, namely, $\{a_n\}$ and $\{b_n\}$ ($n = 1, 2, 3\ldots$), which are proportional to electric and magnetic multipoles radiating from the origin [27]. Specifically, backward (Q_b) and forward (Q_f) scattering efficiencies for a homogeneous sphere with a radius of a under illumination of plane waves are given by [44]

$$Q_b = \frac{1}{k^2 a^2}\left|\sum_{n=1}^{\infty}(2n+1)(-1)^n(a_n - b_n)\right|^2, \quad (6)$$

$$Q_f = \frac{1}{k^2 a^2}\left|\sum_{n=1}^{\infty}(2n+1)(a_n + b_n)\right|^2, \quad (7)$$

where k is the wave number in the host medium. From the two expressions, one can find that Q_b and Q_f can be minimized under certain conditions. For instance, when just considering dipolar contribution (neglecting a_n and b_n, $n \geqslant 2$), if the electric and magnetic dipoles have the same amplitudes and oscillate in phase ($a_1 = b_1$), backward scattering can be completely suppressed. On the contrary, if the two dipoles oscillate out of phase ($a_1 = -b_1$), forward scattering can be totally eliminated. These two circumstances are the well-known first and second Kerker conditions [27,28]. What is more, as the dimension of the two-layered system in this work is of subwavelength, it is reasonable to take the first four Mie coefficients, namely a_1, b_1, a_2, and b_2, into consideration [28]. Based on above discussions, the Electromagnetic Multipole Decomposition Method [45] is integrated into COMSOL MULTIPHYSICS to extract the first four Mie terms in order to reveal the physical insights behind the differences among RCSF$_{norm}$, RCSAv$_{norm}$, and RCSB$_{norm}$ in Fig. 2.

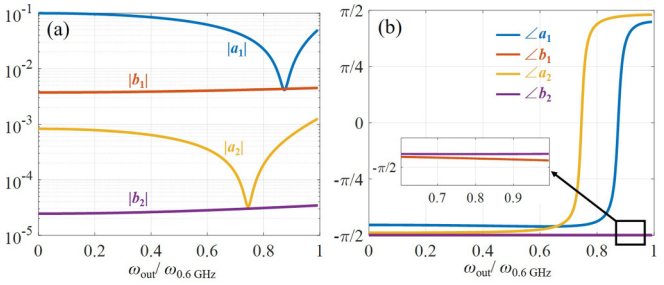

FIG. 4. Amplitudes (a) and phases (b) of a_1, b_1, a_2, and b_2 under different $\omega_{out}/\omega_{0.6\,GHz}$ when $d_{out}/\lambda_{0.6\,GHz} = 0.02$, where blue, orange, yellow, and purple curves correspond to a_1, b_1, a_2, and b_2, respectively.

Without loss of generality, the characteristics of Mie coefficients under different $\omega_{out}/\omega_{0.6\,GHz}$ when $d_{out}/\lambda_{0.6\,GHz} = 0.02$ are analyzed. In the beginning, the amplitudes and phases of a_1, b_1, a_2, and b_2 when varying $\omega_{out}/\omega_{0.6\,GHz}$ are shown in Figs. 4(a) and 4(b). Obviously, first-order Mie coefficients dominate total scattering since ($|a_1|$, $|b_1|$) $\gg$ ($|a_2|$, $|b_2|$). Also, it can be observed that $|a_1|$ has a dip around $\omega_{out}/\omega_{0.6\,GHz} = 0.87$ with the increase of $\omega_{out}/\omega_{0.6\,GHz}$. This is because the underdense outer plasma shell ($\omega_{out}/\omega_{0.6\,GHz} < 1$), compared with the inner overdense one ($\omega_{in}/\omega_{0.6\,GHz} = 3.35$), exhibits a negative polarizability [35–37]. As a result, the total electric dipole element of the system $\mathbf{p}_{tot}$ (proportional to a_1 as $\mathbf{p}_{tot} = \varepsilon_0\alpha_e\mathbf{E}_0$, where $\alpha_e = i6\pi a_1/k^3$) will decline to a minimum when the electric polarization of inner plasma shell and the electrically small antenna is nearly offset by the outer plasma shell. Nonetheless, with the continuous increment of $\omega_{out}/\omega_{0.6\,GHz}$, the excessive offset provided by the outer plasma shell contributes to the augmentation of $|a_1|$ [Fig. 4(a)] and a steep jump of $\angle a_1$ from $\sim -\pi/2$ to $\sim \pi/2$ [Fig. 4(b)]. By contrast, $|b_1|$ and $\angle b_1$ are weakly associated with ω_{out} when $\omega_{out}/\omega_{0.6\,GHz} < 1$. Furthermore, of particular interest is that the amplitudes and phase angles of a_2 and b_2 show similar changes with regard to $\omega_{out}/\omega_{0.6\,GHz}$, though they play a minor role in scattering.

Since a_1 and b_1 dominate total scattering, the connection between RCSF$_{norm}$/RCSAv$_{norm}$/RCSB$_{norm}$ and the imaginary and real parts of a_1 and b_1 under different $\omega_{out}/\omega_{0.6\,GHz}$ ($0.82 \sim 0.92$) is presented in Figs. 5(a) and 5(b). In Fig. 5(b), it can be seen that the imaginary part of b_1 is much larger than

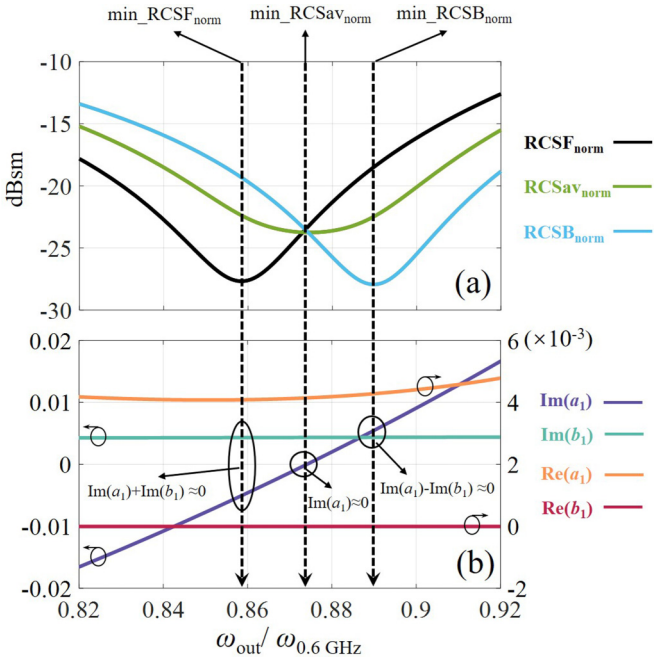

FIG. 5. (a) RCSF$_{norm}$ (black), RCSAv$_{norm}$ (grass green), and RCSB$_{norm}$ (blue) under different $\omega_{out}/\omega_{0.6\,GHz}$ ($0.82 \sim 0.92$). (b) Imaginary and real parts of a_1 and b_1 under different $\omega_{out}/\omega_{0.6\,GHz}$ ($0.82 \sim 0.92$), where purple, dark green, orange, and red curves stand for Im(a_1), Im(b_1), Re(a_1), and Re(b_1); black dashed lines, from left to right, designate positions of min_RCSF$_{norm}$, min_RCSAv$_{norm}$, and min_RCSB$_{norm}$.

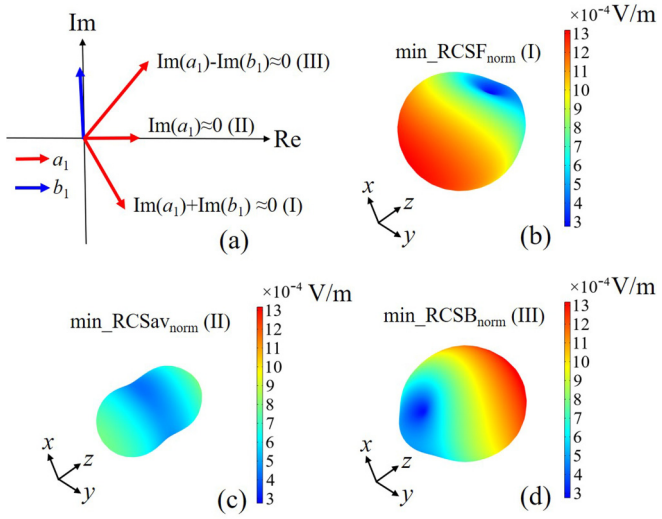

FIG. 6. (a) a_1 (red) and b_1 (blue) in the phase space for Im(a_1) + Im(b_1) ≈ 0 (I), Im(a_1) ≈ 0 (II), and Im(a_1) − Im(b_1) ≈ 0 (III) when $d_{out}/\lambda_{0.6\,GHz} = 0.02$; 3D scattering patterns (norm of electric far field) for (b) min_RCSF$_{norm}$, (c) min_RCSAv$_{norm}$, and (d) min_RCSB$_{norm}$.

the real part, and both of them are hardly changed when varying ω_{out}. For a_1, with the increase of $\omega_{out}/\omega_{0.6\,GHz}$, Im($a_1$) is positively proportional to $\omega_{out}/\omega_{0.6\,GHz}$ and its absolute value reaches a minimum at $\omega_{out}/\omega_{0.6\,GHz} \sim 0.875$, while Re($a_1$) is relatively stable. Also, as illustrated by three black dashed lines, the positions of min_RCSF$_{norm}$, min_RCSAv$_{norm}$, and min_RCSB$_{norm}$ in Fig. 5(a) actually correspond to those of Im(a_1) + Im(b_1) ≈ 0, Im(a_1) ≈ 0, and Im(a_1) − Im(b_1) ≈ 0 in Fig. 5(b), which can be regarded as quasisecond-Kerker condition, plasmonic cloaking, and quasifirst-Kerker condition, respectively, and are more intuitively demonstrated in Fig. 6(a). It should also be noted that the two quasi-Kerker conditions are satisfied near the cutoff band of a_1 ($|a_1| \approx 0$), which guarantees the directional scattering to be tuned with omnidirectional invisibility, as shown in Fig. 2.

Finally, the relationship between a_1 and b_1 in the phase space and corresponding 3D scattering patterns (norm of electric far field) for min_RCSF$_{norm}$, min_RCSAv$_{norm}$, and min_RCSB$_{norm}$ when $d_{out}/\lambda_{0.6\,GHz} = 0.02$ are shown in Fig. 6. It can be observed that when Im(a_1) + Im(b_1) ≈ 0 (case I), the destructive interference between an electric dipole and a magnetic dipole enables the scattering pattern similar to a "Huygens reflector [32]" [Fig. 6(b)]. When Im(a_1) ≈ 0 (case II), the minimal total scattering of the target is achieved, obvious in Fig. 6 as the norm of electric far field in Fig. 6(c) has a minimal peak. This is exactly the principle of plasmonic cloaking. And, when Im(a_1) − Im(b_1) ≈ 0 (case III), the constructive interference between an electric dipole and a magnetic dipole reshapes the scattering pattern parallel to a "Huygens secondary source [32]" [Fig. 6(d)]. Note that it is the mismatch of real parts between a_1 and b_1 [orange and red lines in Fig. 5(b)] that makes the scattering patterns in Figs. 6(b) and 6(d) not identical to those cases with the first and second Kerker conditions rigorously satisfied, as a small protruded scattering component still exists in both forward and backward directions.

IV. CONCLUSION

In conclusion, tunable Kerker-type invisibility and omnidirectional signal enhancement are fulfilled simultaneously at different frequency bands by a core-shell overdense-underdense or ENG-ELP plasma pair. It is shown that the underdense outer plasma shell with a negative polarizability can reduce the intensity of electric dipolar (a_1) response of the system and tune its phase, while the magnetic dipolar term hardly changes. In this case, interference between electric (a_1) and magnetic (b_1) dipolar responses is restricted to the cutoff band of a_1. Further, with the increase of ω_{out}, the nature of interference between electric and magnetic dipolar scattering components alters from destructive to constructive. As a result, quasisecond-Kerker condition, plasmonic cloaking, and quasifirst-Kerker condition can be satisfied in sequence, and correspondingly, min_RCSF$_{norm}$, min_RCSAv$_{norm}$, and min_RCSB$_{norm}$ can be obtained in order. For future experimental investigations, one can use different kinds of plasma generators to fabricate the inner (e.g., inductively coupled plasma) and outer plasma (e.g., DC glow discharge or capacitively coupled plasma) with proper combination in one system.

The data that support the findings of this study are available from the corresponding author upon reasonable request.

ACKNOWLEDGMENT

This work was supported by the National Natural Science Foundation of China (NSFC) under Grants No. 11875118 and No. 52022026.

The authors declare no conflicts of interest.

[1] K. R. Stalder, R. J. Vidmar, and D. J. Eckstrom, J. Appl. Phys. **72**, 5089 (1992).
[2] O. Sakai, T. Sakaguchi, and K. Tachibana, Appl. Phys. Lett. **87**, 241505 (2005).
[3] J. S. Zhao, S. Z. Wang, H. F. Hu, Y. Liu, Y. M. Chang, and X. Q. Chen, Appl. Phys. Lett. **110**, 094108 (2017).
[4] F. R. Kong, Y. F. Sun, S. Lin, Q. Y. Nie, Z. B. Wang, Z. L. Zhang, B. W. Li, and B. H. Jiang, IEEE Trans. Plasma Science. **45**, 381 (2017).
[5] V. Laquerbe, R. Pascaud, A. Laffont, T. Callegari, L. Liard, and O. Pascal, Phys. Plasmas **26**, 033509 (2019).
[6] P. P. Sun, R. Y. Zhang, W. Y. Chen, P. V. Braun, and J. G. Eden, Appl. Phys. Rev. **6**, 041406 (2019).
[7] N. Askari, R. Mirzaie, and E. Eslami, Phys. Plasmas **22**, 112117 (2015).
[8] Y. L. Wang, S. Liu, and S. Y. Zhong, Opt. Commun. **473**, 125985 (2020).
[9] O. Sakai and K. Tachibana, Plasma Sources Sci. Technol. **21**, 013001 (2012).
[10] T. B. Yang, T. Fu, and Y. B. An, Phys. Plasmas **29**, 012103 (2022).
[11] B. Wang and M. A. Cappelli, Appl. Phys. Lett. **107**, 171107 (2015).
[12] H. J. Yang, S. J. Park, and J. G. Eden, J. Phys. D: Appl. Phys. **50**, 43LT05 (2017).
[13] B. Wang and M. A. Cappelli, AIP. Adv. **6**, 065015 (2016).
[14] J. A. Rodríguez, A. I. Abdalla, B. Wang, B. Lou, S. H. Fan, and M. A. Cappelli, Phys. Rev. Appl. **16**, 014023 (2021).
[15] E. Prodan, C. Radloff, N. J. Halas, and P. Nordlander, Science **302**, 419 (2003).
[16] K. L. Kelly, E. Coronado, L. L. Zhao, and G. C. Schatz, J. Phys. Chem. B **107**, 668 (2003).
[17] S. A. Maier, *Plasmonics: Fundamentals and Applications* (Springer, New York, 2007).
[18] A. M. Messiaen and P. E. Vandenplas, Electron. Lett. **3**, 26 (1967).
[19] C. C. Lin and K. M. Chen, IEEE Trans. Antennas Propag. **17**, 675 (1969).
[20] R. W. Ziolkowski and A. D. Kipple, Phys. Rev. E **72**, 036602 (2005).
[21] C. Pfeiffer and A. Grbic, IEEE Trans. Antennas Propag. **60**, 1671 (2012).
[22] C. S. Wang, H. Liu, X. A. Li, and B. H. Jiang, Phys. Plasmas **22**, 063501 (2015).
[23] B. W. Li, Q. Y. Nie, X. G. Wang, S. Lin, P. Q. Chen, and B. N. Qu, Phys. Plasmas **27**, 040701 (2020).
[24] A. Laffont, R. Pascaud, T. Callegari, L. Liard, O. Pascal, and J. Adam, Phys. Plasmas **28**, 033503 (2021).
[25] W. Liu and Y. S. Kivshar, Opt. Express **26**, 13085 (2018).
[26] N. N. Li, Y. H. Lai, S. H. Lam, H. Y. Bai, L. Shao, and J. F. Wang, Adv. Optical Mater. **9**, 2001081 (2021).
[27] M. Kerker, D. S. Wang, and C. L. Giles, J. Opt. Soc. Am. **73**, 765 (1983).
[28] J. M. Geffrin, B. García-Cámara, R. Gómez-Medina, P. Albella, L. S. Froufe-Pérez, C. Eyraud, A. Litman, R. Vaillon, F. González, M. Nieto-Vesperinas, J. J. Sáenz, and F. Moreno, Nat. Commun. **3**, 1171 (2012).
[29] Y. H. Fu, A. I. Kuznetsov, A. E. Miroshnichenko, Y. F. Yu, and B. Luk'yanchuk, Nat. Commun. **4**, 1527 (2013).
[30] W. Liu, A. E. Miroshnichenko, D. N. Neshev, and Y. S. Kivshar, ACS Nano **6**, 5489 (2012).
[31] W. Liu, A. E. Miroshnichenko, D. N. Neshev, and Y. S. Kivshar, Phys. Rev. B **86**, 081407(R) (2012).
[32] S. Lepeshov, A. Krasnok, and A. Alù, ACS Photonics **6**, 2126 (2019).
[33] G. P. Zouros, G. D. Kolezas, E. Almpanis, and K. L. Tsakmakidis, ACS Photonics **8**, 1407 (2021).
[34] T. Naito, T. Tanaka, Y. Fukuma, and O. Sakai, Phys. Rev. E **99**, 013204 (2019).
[35] P. Q. Chen, Q. Y. Nie, Z. L. Zhang, B. W. Li, S. Lin, and B. N. Qu, Phys. Plasmas **27**, 053502 (2020).
[36] A. Alù and N. Engheta, Phys. Rev. E **72**, 016623 (2005).
[37] A. Alù and N. Engheta, Opt. Express **15**, 3318 (2007).
[38] A. Alù and N. Engheta, Phys. Rev. E **78**, 045602(R) (2008).
[39] S. Tricarico, F. Bilotti, A. Alù, and L. Vegni, Phys. Rev. E **81**, 026602 (2010).
[40] B. Edwards, A. Alù, M. G. Silveirinha, and N. Engheta, Phys. Rev. Lett. **103**, 153901 (2009).
[41] H. Singh, S. Antony, and R. M. Jha, *Plasma-based Radar Cross Section Reduction* (Springer, Singapore, 2016).
[42] COMSOL Multiphysics, http://www.comsol.com/
[43] C. F. Bohren and D. R. Huffman, *Absorption and Scattering of Light by Small Particles* (Wiley, New York, 1983).
[44] B. luk'yanchuk, N. I. Zheludev, S. A. Maier, N. J. Halas, P. Nordlander, H. Giessen, and C. T. Chong, Nat. Mater. **9**, 707 (2010).
[45] P. Grahn, A. Shevchenko, and M. Kaivola, New J. Phys. **14**, 093033 (2012).